SECOND EUROPEAN CONFERENCE ON EARTHQUAKE ENGINEERING
AND SEISMOLOGY, ISTANBUL AUG. 25-29, 2014

REVIEW AND IMPROVEMENT OF SIMPLE MECHANICAL MODELS FOR PREDICTING THE FORCE-DISPLACEMENT RESPONSE OF URM WALLS SUBJECTED TO IN-PLANE LOADING

Sarah PETRY[1] and Katrin BEYER[2]

ABSTRACT

In performance-based seismic design the global displacement capacity of structures is predicted on the basis of local engineering demand parameters and mechanical models that link local and global deformation quantities. Although unreinforced masonry (URM) is one of the most used construction materials for residential structures all over the world, the displacement capacity of in-plane loaded URM walls is still mainly estimated from empirical drift capacity models rather than mechanical relationships between local and global deformation capacities.

In this article, we present an analytical model which links the top displacement of an URM wall to the applied in-plane shear load. In order to verify the model, we compare the predicted results to global and local deformation quantities from own URM wall tests. Comparison of global deformation quantities shows that we are able to predict the initial stiffness of the walls with the simple assumption of a no-tension material and a linear-elastic material in compression. For walls developing a diagonal shear failure or hybrid failure, the predicted force-displacement curve starts diverging from the experimental envelope with the formation of the first diagonal cracks. With comparison of local deformation quantities, e.g. curvature profiles and shear strain profiles, we show that this is due to the formation of a significant diagonal shear crack.

INTRODUCTION

In performance-based seismic design the global displacement capacity of structures is predicted on the basis of local performance levels and mechanical models that link local and global deformation quantities. Although unreinforced masonry (URM) is one of the most commonly used construction materials for residential structures all over the world, the displacement capacity of in-plane loaded URM walls is still mainly estimated from empirical drift capacity models (e.g. CEN, 2005) rather than mechanical relationships between local and global deformation capacities. Already some decades ago,

[1] Sarah Petry, Earthquake Engineering and Structural Dynamics (EESD), School of Architectural, Civil and Environmental Engineering (ENAC), École Polytechnique Fédérale de Lausanne (EPFL), sarah.petry@epfl.ch

[2] Katrin Beyer, Earthquake Engineering and Structural Dynamics (EESD), School of Architectural, Civil and Environmental Engineering (ENAC), École Polytechnique Fédérale de Lausanne (EPFL), katrin.beyer@epfl.ch

first models were developed which aimed at describing the force-displacement relationship of unreinforced masonry (URM) structures subjected to in-plane loading. Some are of analytical nature and develop a direct relationship between lateral force and top displacement. Examples of such models are for instance, the force-displacement relationship for leaning towers (Heyman, 1992) or the analytical force-displacement relationship for rocking walls developed by Benedetti and Steli (2008). Other models allow obtaining the force-displacement relationship with the help of computer software in form of macro-elements (e.g. Penna et al., 2013).

All these models share the assumption that the masonry behaves linearly in compression and cannot transmit tension. Hence, for small lateral loads the wall behaves linear-elastically until the onset of decompression at the base of the wall when a horizontal crack starts opening up (Fig. 1, $V \leq V_e$). In the following, the effective section reduces and the flexibility of the wall increases (Fig. 1, $V > V_e$). Considering the reduced area, the curvature and the shear strain are estimated and both quantities can be integrated in order to obtain flexural and shear displacement. Thus, the force-displacement relationship can be obtained.

This article builds on the model by Benedetti and Steli (2008) and expands this in two principal points: (i) first, we account for the reduction of the compressed cross section also when computing the shear deformations; (ii) second, the model is extended for walls with boundary conditions different to those of cantilever walls or fixed-fixed conditions.

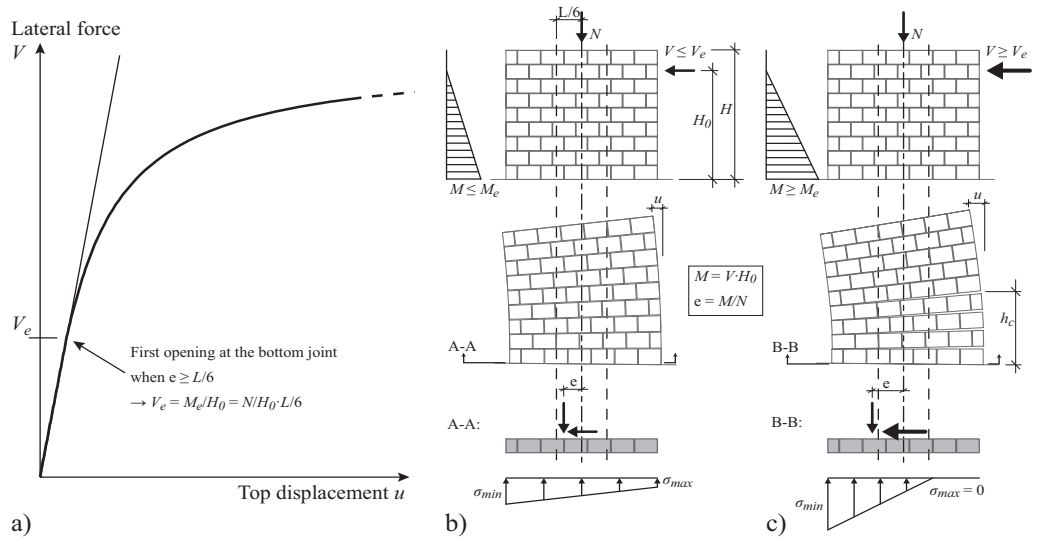

Figure 1. a) Force-displacement relationship for a no-tension material with linear-elastic behaviour in compression, b) behaviour before the onset of decompression and c) behaviour after decompression

MODEL FOR THE FORCE-DISPLACEMENT BEHAVIOUR OF URM WALLS

In Benedetti and Steli (2008) a model is developed which aims at describing the direct relationship between the top displacement and the applied lateral load of URM walls solicited mainly to flexural deformations. Based on the model by Benedetti and Steli (2008), in Petry and Beyer (2014a) a reviewed model is proposed which regards the deformation quantities due to shear and flexure separately and is thus able to account for the non-linearity of both deformation quantities. Furthermore, the model is extended for a variable shear span ratio. Hence, the following relationship is obtained between the applied lateral load and the displacement u_{fl} due to flexural solicitation (Petry and Beyer, 2014a):

$$u_{fl} = V \cdot \frac{H^3}{2EI}\left(\alpha - \frac{1}{3}\right) \qquad \text{for } V \leq V_e \qquad (1)$$

$$u_{fl} = u_{e,fl} \cdot \left(\left(1 - \frac{\alpha^2 (3-\alpha)}{3\alpha - 1} \right) \cdot \frac{V}{V_e} + \frac{3\alpha^2 (1-\alpha)}{3\alpha - 1} \cdot \frac{V_e}{V} + \frac{2\alpha^3}{3\alpha - 1} \cdot \left(\frac{V_e}{V} \right)^2 \right) + \theta(V) \cdot \left(H(1-\alpha) + \frac{M_e}{V} \right) + \psi(V) \quad \text{for } V > V_e \tag{2}$$

with

$$\theta(V) = -\frac{2N^2}{9ETLV}(\mu - 6\eta) \tag{3}$$

$$\psi(V) = -\frac{N^3}{9ETV^2}\left(\frac{2}{3}\mu - 4\eta + 2\ln\left(\frac{2}{3}\mu \right) \right) \tag{4}$$

$$\mu = \frac{L \cdot N}{L \cdot N - 2\alpha H \cdot V} \tag{5}$$

$$\eta = \frac{\alpha H \cdot V}{L \cdot N - 2\alpha H \cdot V} \tag{6}$$

where L, T and H are the length, thickness and height of the wall. E is the E-modulus, and $I = L^3T/12$ is the inertia. N is the applied axial load, V the shear load and α the ratio between shear span H_0 and height of the wall H. $u_{e,fl}$ is the flexural displacement at the onset of decompression ($V = V_e$).

When we consider a wall that is mainly subjected to flexural deformations, we assume that damage to the wall is only introduced through flexural deformations. Nevertheless, the shear deformations cannot be neglected and similar to the flexural stiffness; the shear stiffness reduces with the reduction of the effective area. Hence, the shear deformation can be divided into two domains. In the first domain, when the whole section of the wall is in compression (see Fig. 1, $V \leq V_e$), the shear deformations are independent of the moment profile of the wall and the shear displacement can be described as follows:

$$u_{sh} = V \cdot \frac{5H}{6GA} \quad \text{for } V \leq V_e \tag{7}$$

where G is the shear modulus and $A = TL$ the area of the full section.

When the bottom joint starts opening, the effective area through which the shear stress is transferred reduces. Thus, the deformability increases and the following force-shear displacement relationship is obtained:

$$u_{sh} = u_{e,sh} \cdot \left(\alpha + \frac{V}{V_e}(1-\alpha) \right) + \psi_{sh}(V) \quad \text{for } V > V_e \tag{8}$$

with

$$\psi_{sh}(V) = \frac{5N}{18GT} \cdot \ln\left(\frac{2}{3}\mu \right) \tag{9}$$

$$\mu = \frac{L \cdot N}{L \cdot N - 2\alpha H \cdot V} \tag{10}$$

where $u_{e,sh}$ is the shear displacement at the onset of decompression ($V = V_e$).

The total displacement u_{tot} is obtained as sum of both deformation quantities:

$$u_{tot} = u_{fl} + u_{sh} \tag{11}$$

EXPERIMENTS ON FIVE URM WALLS FOR COMPARISON

In order to investigate the influence of the boundary conditions on URM walls, we tested six walls under a cyclic quasi-static lateral force in in-plane direction in the structural laboratory of the EPF Lausanne, Switzerland. All walls were identical to each other with the dimensions of L x H x T = 2.01 x 2.25 x 0.20 m and the tests varied between each other by means of the applied boundary conditions, hence, axial stress ratio σ_0/f_u and shear span ratio $\alpha = H_0/H$. For the first five walls the axial stress ratio was kept constant at σ_0/f_u = 0.09, 0.18 or 0.26 respectively, where σ_0 is the applied mean axial stress and f_u the compression strength of the masonry, while the shear span was kept constant at H_0 = 0.5, 0.75 to 1.5, respectively, times the wall height H. The applied boundary conditions for the first five specimens can be taken from Table 1. The boundary conditions for the last wall, PUP6, were particular and this wall is therefore not discussed herein this paper. The resulting failure mechanisms and drift capacity of all walls are summarized in Table 2. More information on the test programme and material properties can be taken from Petry and Beyer (2013; 2014b). During testing, we tracked with a set of cameras the displacement of four LEDs on each full brick of the masonry walls. Therefore, we were able to determine the local deformations, e.g., average strains in the bricks and deformations in the joints, and put these local measures in relationship to global displacement capacities.

However, the results showed that despite what most codes assume (see Table 2), e.g., Eurocode 8 – Part 3 (CEN, 2005), the displacement capacity is not constant for the same failure mode (Petry and Beyer, 2014b), but depends on the boundary conditions and other factors. In Petry and Beyer (2014c) we show that this is due to the fact that even though a clear failure mechanism can be associated to four out of the five walls, all walls developed damage patterns typical for flexural and shear solicitation.

Petry and Beyer (2014c) identify five different damage levels for each of the two typical failure modes, diagonal shear and flexural rocking, and link these to different limit states of the global force-displacement response of URM walls. The limit states for flexural deformation reach from LS-F1, which represents the first appearance of a crack in the horizontal joints and is associated to a first reduction of the stiffness, to LS-F5 which is associated to the collapse of the base zone and is thus linked to the loss of axial load capacity. The limit states for shear failure reach from LS-S1, which represents the first appearance of a diagonal crack in joints and is associated with a first softening of the global force-displacement curve, to LS-S5, which represents the state when the diagonal crushes completely and the wall cannot sustain the applied axial load any longer.

Table 1. Boundary conditions for PUP1-5 (Petry and Beyer 2014c)

σ_0/fu ; H_0/H	0.5	0.75	1.5
0.09	-	PUP5	-
0.18	PUP1	PUP2	PUP3
0.26	-	-	PUP4

Table 2. Failure modes and ultimate drift capacity in dependency of the applied boundary conditions (Petry and Beyer 2014c)

σ_0/fu ; H_0/H	0.5	0.75	1.5
0.09	-	Diagonal shear 0.54 %	-
0.18	Diagonal shear 0.17 %	Diagonal shear 0.40 %	Flexural rocking 0.72 %
0.26	-	-	Hybrid 0.35 %

PREDICTION OF THE FORCE-DISPLACEMENT RELATIONSHIP

In Fig. 2, the model from Petry and Beyer (2014a) is used to predict the force-displacement relationship of the URM walls from the PUP-series. Comparison of the first loading envelopes with the prediction of the model shows that the model predicts well the initial stiffness of all walls. When the failure mode of the wall is dominated by flexural rocking (PUP3 and PUP4), the mechanical model can further predict the force-displacement relationship until first significant damage is introduced to the walls. However, if a significant diagonal shear mechanism develops, model and experimental results start to diverge from an early stage on and for the walls PUP1, PUP2 and PUP5 the model overestimates the stiffness already before first diagonal cracks were visible.

In the following we show the different local deformation measures and compare these to the quantities assumed in the model. These are the effective reduction of contributing section in the base section and deformation profiles (curvature and shear strains) measured in the compressed part of the walls. Based on these local comparisons we discuss the validity of the basic assumption on which the model is based and thus its limitation and possible improvements.

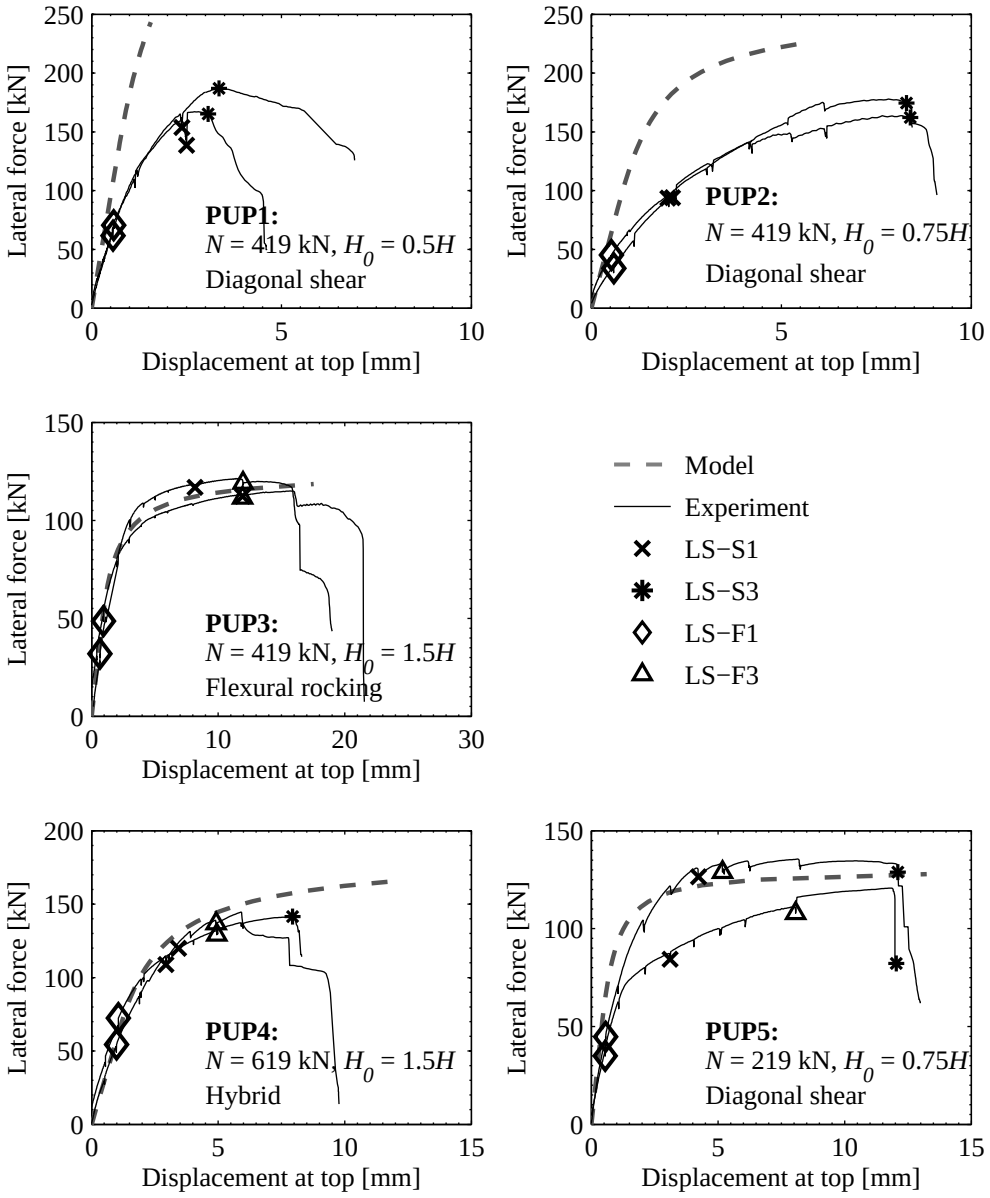

Figure 2. Force-displacement relationship for a no-tension material with linear-elastic behaviour in compression

COMPARISON OF MODEL WITH EXPERIMENTS AT LOCAL LEVEL

The model developed in Benedetti and Steli (2008) and Petry and Beyer (2014a) is based on the assumption that masonry cannot transmit tension perpendicular to the bed joints. Hence, at the onset of decompression the horizontal joints open up and cause a reduction of the contributing area. This reduction of the contributing area can be expressed by means of the compression length, which varies over the height of the wall. In Fig. 3 the measured compression length ratio L_c/L in the base section is shown versus the moment in base.

In the model the reduction of the compressed area is estimated assuming a plane remaining section and linear-elastic behaviour of the masonry in compression. Hence, the following equations are used for computing the compression length L_c:

$$L_c = L \qquad \text{for } V \leq V_e \qquad (12)$$

$$L_c = 3\left(\frac{L}{2} - \frac{M}{N}\right) \qquad \text{for } V > V_e \qquad (13)$$

where L is the length of the wall, M the moment in the base section and N the applied axial load.

From Fig. 3 it can be noted that the best match between model and experiment is obtained for the walls PUP3-5 where flexural deformations were largest. For PUP1 and PUP2 the moment demand is too small to develop significant cracks in the base joint.

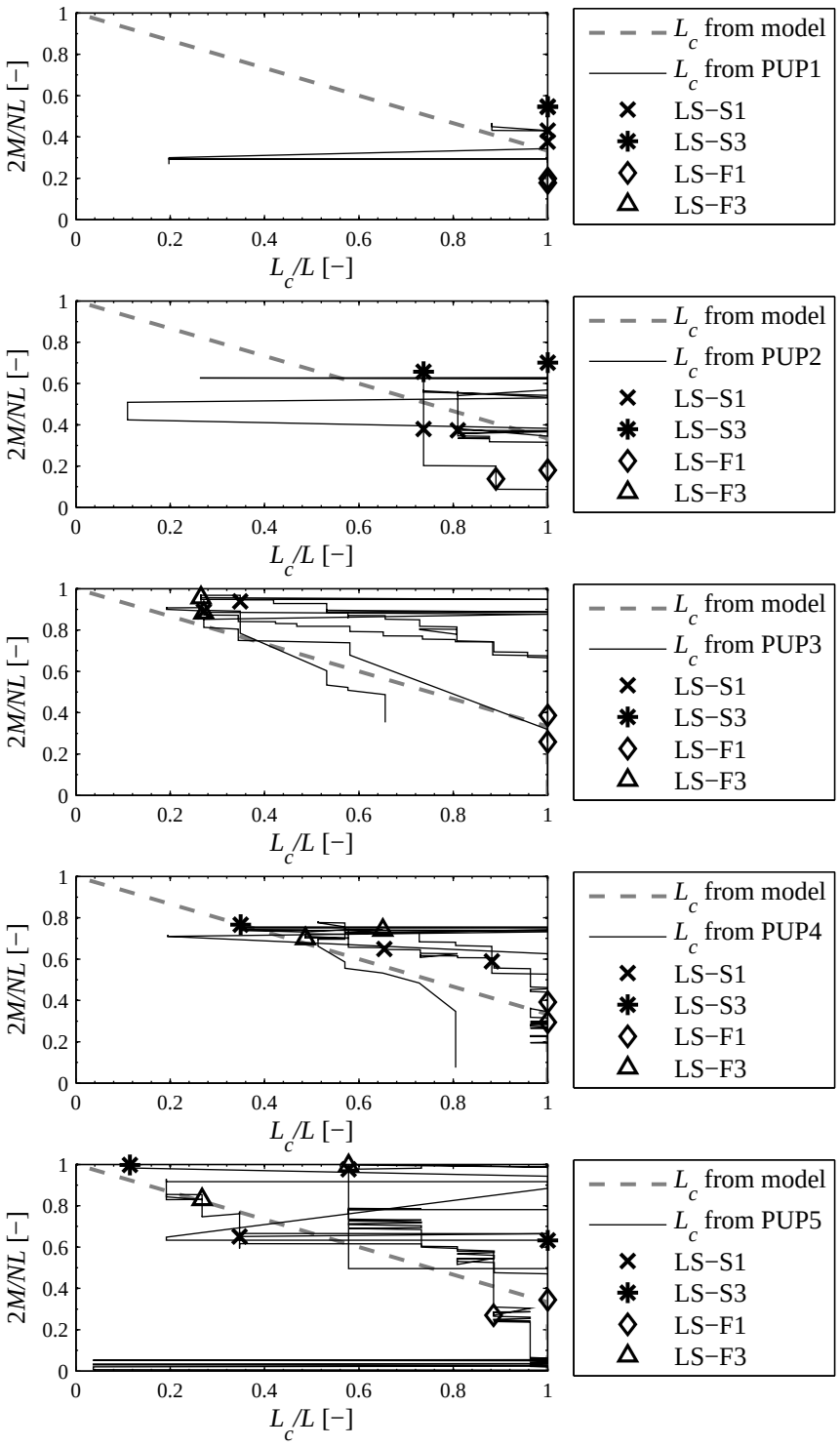

Figure 3. Compressed portion L_c/L in base joint versus normalized based moment $2M/NL$

Based on the reduced area, the model computes the flexural displacement from the double integration of the curvature and the shear displacement from the integration of the shear strain. In order to verify both quantities we compute curvature and shear strains from the deformation measurements of the walls and compare them to the assumed strain and curvature profiles. In Fig. 4 the curvature profiles are plotted for the limit states LS-F3, LS-S1 and LS-S3 (see Fig. 1). The curvatures from experiments are obtained as outlined in Petry and Beyer (2014c), i.e., only the deformations of the compressed wall part are used to derive the curvatures from the experimental results.

In the model the curvature is computed assuming plane sections remaining plane and a linear-elastically behaviour in compression. Hence,

$$\chi = \frac{12M}{ETL^3} \qquad \text{for } V \leq V_e \qquad (14)$$

$$\chi = \frac{2N}{ETL_c^{\,2}} \qquad \text{for } V > V_e \qquad (15)$$

where L and T are the length and thickness of the wall, E is the E-modulus of the masonry, L_c the length of the compression zone computed with Eq. (13) and M the moment of the corresponding section (note that the moment changes with the height).

Comparison of the curvature obtained from experimental results with the curvature obtained from the model shows that the best match is obtained for walls PUP3 and PUP4 (see Fig. 4). Both walls developed a significant flexural behaviour (e.g. Fig. 2, LS-F3) before a significant diagonal shear crack developed. In Petry and Beyer (2014c) we observed that this opening of a significant diagonal crack (LS-S3) in the wall causes the wall to separate into two triangles. Hence, the assumption that plane sections remain plane does not hold any longer and significant differences between experimental results can be observed. This separation of the wall into two triangles introduces also a softening in the walls which is not captured by the model (see Fig. 2).

In Fig. 5 the shear strain profiles are estimated for the limit states LS-F3, LS-S1 and LS-S3 (see Fig. 2). The shear strains from experiments are obtained as average of the shear strains in one section of the strains computed between two layers of bricks. For the same reason as previously stated only the strains measured in the part of the wall which is in compression are used for the curvature. In the model the following relationship between shear force and shear strains is used:

$$\gamma = \frac{5V}{6GTL} \qquad \text{for } V \leq V_e \qquad (16)$$

$$\gamma = \frac{5V}{6GTL_c} \qquad \text{for } V > V_e \qquad (17)$$

where L and T are the length and thickness of the wall and G the shear modulus of the masonry. It is estimated at 40% of E.

In Fig. 5 the same tendency is observed as for the curvature. While for the walls dominated by a flexural behaviour the model gives a good estimate for the shear strains, e.g., PUP3 and PUP4, for the other walls the shear strains are considerably underestimated. As stated previously, the opening of a significant diagonal shear crack (LS-F3) provokes the wall to separate in two independent triangles. These two triangles are more flexible than an equivalent rectangular wall.

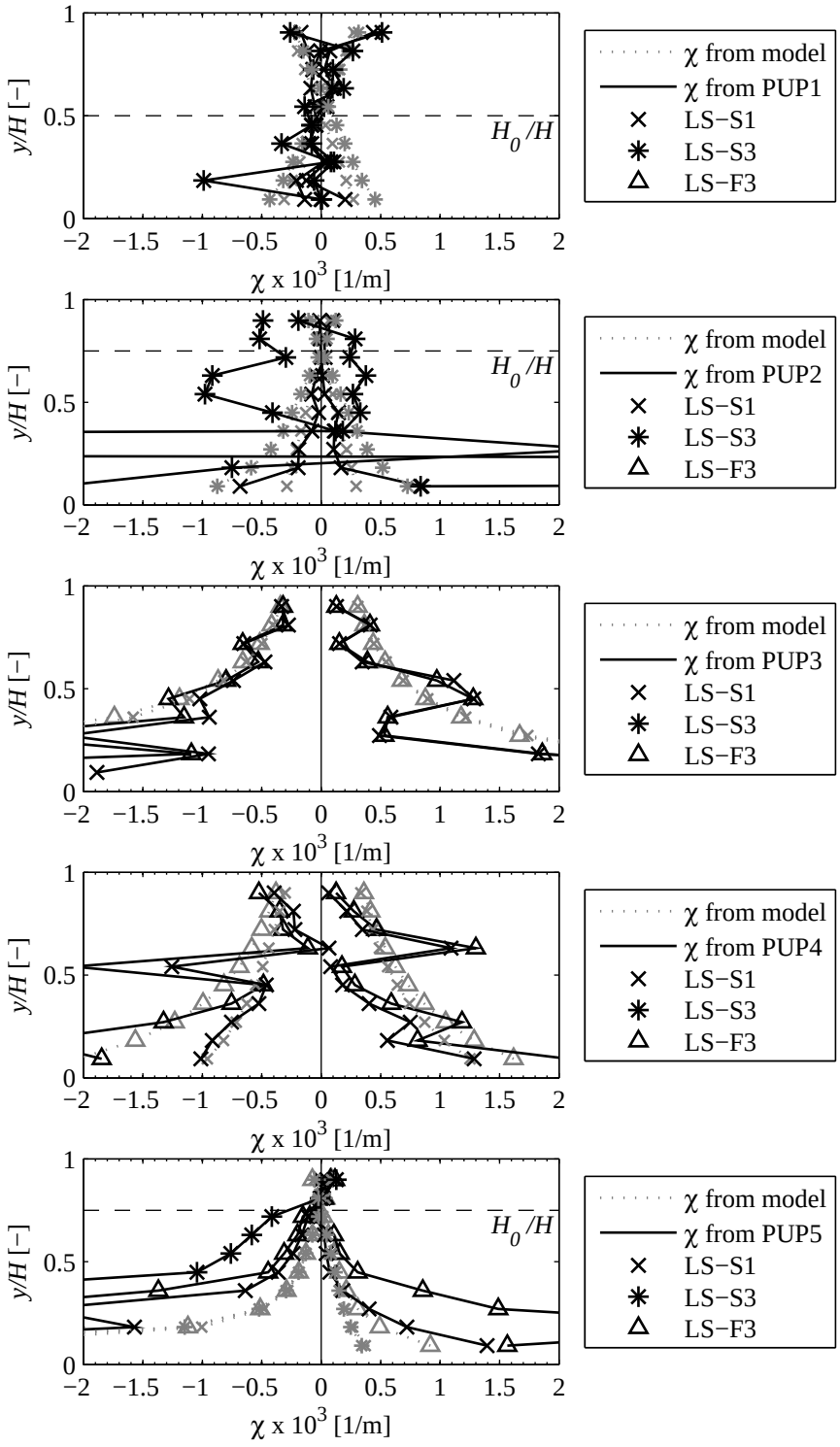

Figure 4. Curvature profiles for the limits states LS-S1, LS-S3 and LS-F3

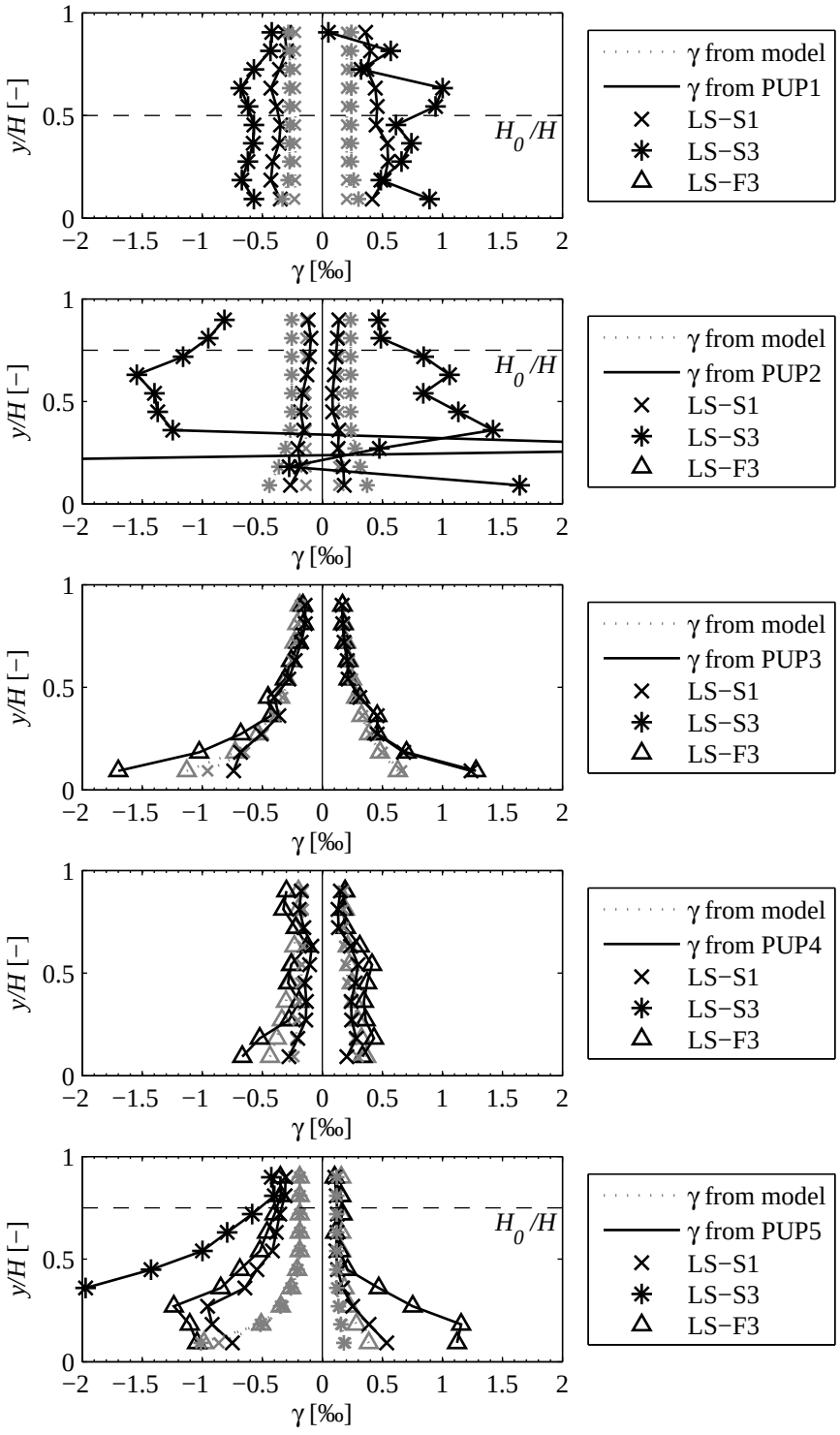

Figure 5. Shear strain profiles for the limits states LS-S1, LS-S3 and LS-F3

CONCLUSIONS

In this article, we present an analytical model which links the top displacement of an unreinforced masonry (URM) wall to the applied in-plane shear load. In order to verify the model, we compare the predicted results to own URM wall tests. We tested several identical URM walls under different constant axial load N and shear span ratios H_0/H, while applying a quasi-static cyclic horizontal load (test units PUP1-5). During testing, we tracked with a set of cameras the displacement of four LEDs on each full brick of the masonry walls. Therefore, we were able to determine the local deformations, e.g., average strains in the bricks and deformations in the joints, and put these local measures in relationship to global displacement capacities. Comparison of global deformation quantities shows that we are able to predict the initial stiffness of the walls with the simple assumption of a no-tension material and a linear-elastic material in compression. When the failure mode of the wall is dominated by flexural rocking, the mechanical model can further predict the force-displacement capacity until significant damage is introduced to the walls. For walls developing a diagonal shear failure or hybrid failure, the predicted force-displacement curve starts diverging from the experimental envelope with the formation of the first diagonal cracks. This is due to the fact that once diagonal cracks start forming in the centre of the wall, the assumption of a plane remaining sections does no longer hold. The diagonal crack provokes the wall to separate into two triangles and thus, softens the wall.

Therefore, we are currently working on the herein presented model in order to improve it in two aspects. First, we are developing a failure criterion in order to link local deformation limits in the toe and in the centre crack of the wall to the global displacement capacity; second we are working on the implementation of a model, which can account for the opening of the diagonal shear crack in order to model the softening observed during the experiments and shear failure.

REFERENCES

CEN (2005) Eurocode 8: Design of structures for earthquake resistance – Part 3: assessment and retrofitting of buildings, Design Code EN 1998-3, European Committee for Standardisation (CEN), Brussels, Belgium

Benedetti A and Steli E (2008) “Analytical models for shear-displacement curves of unreinforced and FRP reinforced masonry panels,” *Construction and Buildings Materials*, 22: 175-185

Heyman J (1992) “Leaning towers,” *Meccanica*, 27: 153-159

Penna A, Lagomarsino S and Galasco A (2013) “A nonlinear macroelement model for the seismic analysis of masonry buildings,” *Earthquake Engineering and Structural Dynamics*, DOI: 10.1002/eqe.2335

Petry S and Beyer K (2013) “Cyclic test data of six unreinforced masonry walls with different boundary conditions,” *Submitted in Earthquake Spectra October 2013*

Petry S and Beyer K (2014a) “Force-displacement relationship for in-plane loaded URM walls,” *To be submitted*

Petry S and Beyer K (2014b) “Influence of boundary conditions and size effect on the drift capacity of URM walls,” *Engineering Structure*, 65: 76-88. DOI: 10.1016/j.engstruct.2014.01.048

Petry S and Beyer K (2014c) “Limit states of URM walls subjected to seismic in-plane loading,” *Submitted to Bulletin of Earthquake Engineering February 2014*